NANO LETTERS
Cite This: Nano Lett. XXXX, XXX, XXX−XXX
Letter
pubs.acs.org/NanoLett

Porous Zero-Mode Waveguides for Picogram-Level DNA Capture

Vivek Jadhav,[†] David P. Hoogerheide,[§] Jonas Korlach,[∥] and Meni Wanunu*[,†,‡]

[†]Department of Physics and [‡]Department of Chemistry and Chemical Biology, Northeastern University, Boston, Massachusetts 02115, United States

[§]Center for Neutron Research, National Institute of Standards and Technology, Gaithersburg, Maryland 20899, United States

[∥]Pacific Biosciences, Menlo Park, California 94025, United States

Supporting Information

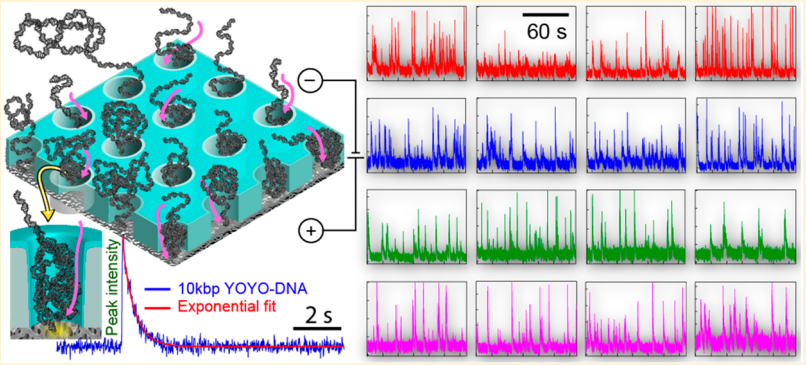

ABSTRACT: We have recently shown that nanopore zero-mode waveguides are effective tools for capturing picogram levels of long DNA fragments for single-molecule DNA sequencing. Despite these key advantages, the manufacturing of large arrays is not practical due to the need for serial nanopore fabrication. To overcome this challenge, we have developed an approach for the wafer-scale fabrication of waveguide arrays on low-cost porous membranes, which are deposited using molecular-layer deposition. The membrane at each waveguide base contains a network of serpentine pores that allows for efficient electrophoretic DNA capture at picogram levels while eliminating the need for prohibitive serial pore milling. Here, we show that the loading efficiency of these porous waveguides is up to 2 orders of magnitude greater than their nanopore predecessors. This new device facilitates the scaling-up of the process, greatly reducing the cost and effort of manufacturing. Furthermore, the porous zero-mode waveguides can be used for applications that benefit from low-input single-molecule real-time sequencing.

KEYWORDS: *Nanopore, nanofabrication, ZMWs, SMRT sequencing, porous membrane*

Over the past few decades, researchers have put tremendous effort into developing new methods for low-cost, high-throughput DNA-sequencing methods.[1−4] Because sequencing is indispensable for probing a variety of genomic characteristics, the revolution sparked by second-generation sequencing (SGS) methods has led to unprecedented growth in the fields of genomic research, clinical diagnostics, and personalized medicine.[5,6] Some limitations of SGS include short read lengths,[7] short consensus assembly, and amplification bias.[8] Recent developments in the sequencing of individual DNA molecules have alleviated some of the drawbacks of SGS methods. In so-called third-generation sequencing (TGS) platforms, individual DNA molecules are read in each sensor, which offers longer median read lengths, consensus maps that are orders of magnitude longer[9] than SGS methods, and the ability to directly detect epigenetic modifications (e.g., base methylation) in native DNA molecules.[10,11] A pair of notable examples of mature TGS methods include nanopore-based sequencing[12,13] and single molecule, real-time (SMRT) sequencing.[3]

In nanopore-based sequencing, ion current through a nanopore embedded in a membrane is read out during the passage of DNA molecules, and the local base sequence of the DNA strand is read out. Using this method, long reads lengths of 882 kb (N50 > 100 kb)[14] were obtained, and the sequencing and assembly of complete microbial genomes (500 Mb to 2 Gb) have been demonstrated.[15−17] More recently, nanopore sequencing was successfully used for challenging projects, such as sequencing and fully assembling the human Y-chromosome.[18,19]

In SMRT sequencing, a DNA-polymerase complex is immobilized by biotin−streptavidin coupling at the bottom of nanowells (100 nm diameter) called zero-mode waveguides (ZMWs).[20] The ZMWs are produced in a 100 nm thick aluminum film deposited on a fused silica substrate.[21] These ZMWs are ordered in dense arrays, each having a zeptoliter-

Received: October 17, 2018
Revised: November 22, 2018
Published: November 28, 2018

DOI: 10.1021/acs.nanolett.8b04170
Nano Lett. XXXX, XXX, XXX−XXX

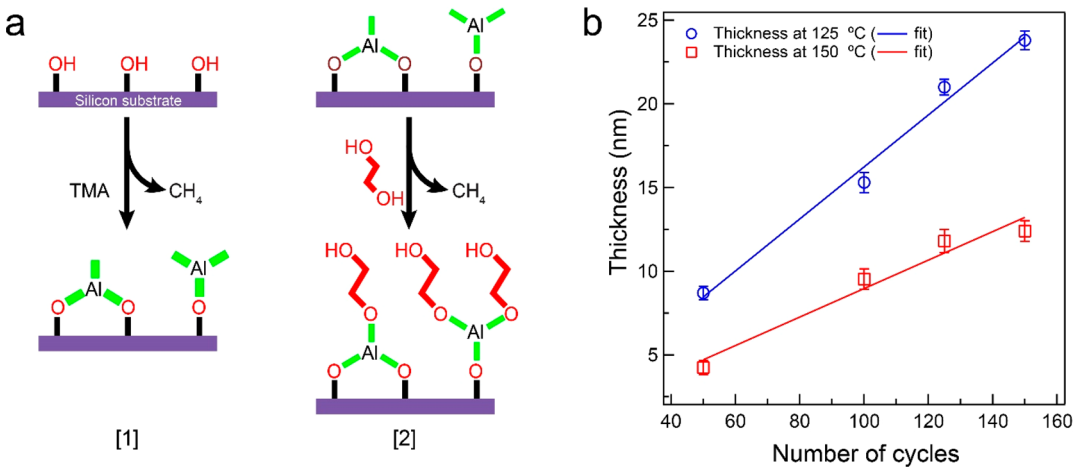

Figure 1. Porous membranes for electrokinetic biomolecular capture. (a) Illustration of the surface chemistry of molecular layer deposition (MLD) using trimethylaluminum (TMA) and ethylene glycol (EG). TMA is deposited on the native hydroxy surface of silicon nitride releasing CH_4 as a byproduct [1], further exposing the surface to EG releasing CH_4 as a byproduct, leaving the surface covered with hydroxylated groups [2]. (b) Thickness measurement of the hybrid organic−inorganic thin film using an ellipsometer as a function of a number of cycles for the same deposition temperature (error bars represent 1 standard deviation from 8 different samples deposited individually).

scale volume. A DNA polymerase that is linked to the base of the ZMWs is used to replicate a DNA fragment, observed in real-time using fluorescently tagged DNA base analogs. The dyes provide a 5−50 ms burst of fluorescence during the incorporation of a Watson−Crick base followed by their diffusion away from the ZMW. Emission from each ZMW is recorded using an optical microscope by wide-field laser excitation of the ZMW bases, and a time series was recorded using an electron-multiplying CCD (emCCD) camera. SMRT sequencing offers maximum read lengths in excess of 60 kb,[22,23] a N50 read length of 19 kb, and a contiguous N50 of 26.9 Mb[24] and has virtually no GC bias.[25] SMRT sequencing has been used to produce accurate *de novo* assemblies of microbial,[26] human,[24] and plant genomes;[27−29] to reconstruct animal genomes;[23] and to uncover human genome structural variation.[30−35]

One challenge in SMRT sequencing is that DNA template loading suffers from steric and entropic limitations due to the ∼100 nm ZMW confinement. In diffusion-based loading, shorter DNA molecules (approximately a few kilobase pairs) are typically captured more efficiently than longer molecules (>10 kbp), resulting in read length bias in a typical sequencing library that contains fragments of various lengths. While a magnetic bead assay[36] has been developed to improve loading efficiencies by 1−2 orders of magnitude, capturing very long DNAs (>10 kbp) is still inefficient, and furthermore, multinanogram-input DNA levels are required. To overcome this, we have recently developed nanopore ZMWs (NZMWs), in which ZMWs are fabricated on top of a freestanding silicon nitride (SiN) membrane, and nanopores are fabricated at the ZMW base to allow voltage-driven electrokinetic DNA capture.[37] We have shown that DNA loading is enhanced by several orders of magnitude when a voltage is applied across a NZMW. This free-standing SiN membrane is mechanically stable and has a high inherent photoluminescence (PL) background. The PL background from the SiN membrane was reduced by fabricating the ZMWs on a 20 nm thick silicon oxide (SiO_2) film atop SiN, then back-etching the photoluminescent nitride layer using reactive ion etching (RIE), resulting in a sufficiently low PL from the free-standing SiO_2 membrane. Using NZMWs, long DNA fragments can be efficiently captured and sequenced using SMRT sequencing.[38] These loading improvements can, when maturing to a practical device, benefit applications in which the analysis of precious samples at picogram levels is needed. However, one drawback of NZMWs is that fabricating massively parallel arrays of nanopores is prohibitively expensive and impractical despite various nanopore-arraying methods that have been developed recently.[39−46]

Because a voltage-biased nanopore acts merely to attract DNA via the electric fields arising from its ion conductivity, we bypass here the need for making individual nanopores by developing a scalable process for hosting a novel porous membrane at the bases of the ZMWs. The porous layer can transport ions through it, yet it does not allow DNA transport across it, resulting in efficient electrokinetic capture. We report here on the properties of this porous layer, also demonstrating the parallel capture of biomolecules from hundreds of ZMWs simultaneously. Our results pave the way for sequencing DNA from picogram levels of input.

Porous Inorganic Films. We have used molecular-layer deposition (MLD)[47,48] to deposit an ultrathin film with controllable film thickness in the nanometer range on SiN, a sacrificial membrane support material. The film was deposited by sequential deposition of trimethylaluminum (TMA) and ethylene glycol (EG) using an atomic-layer deposition (ALD, Arradiance GEMStar) tool (see Figure 1a). The resulting film contains a hybrid organic−inorganic network, so-called alucone,[49,50] the organic component of which disintegrates when immersed in water at room temperature to produce the porous inorganic aluminum oxide network.[51] A schematic illustrating the deposition, borrowed from Miller et al.,[50] is shown in Figure 1a. The precursors TMA and EG were alternately injected, exposing the hydroxylated silicon surface to TMA, which reacts with the surface (Figure 1a-1), releasing methane as the byproduct that is purged out. The surface is later exposed to EG, which binds the accessible functional sites and regenerates hydroxyl functional groups for the next TMA exposure (Figure 1a-2). Thus, by repeating the sequence of TMA and EG, the alucone film was grown to the desired thickness. The alucone thin films of varying thicknesses were deposited on top of the silicon substrate at different

DOI: 10.1021/acs.nanolett.8b04170
Nano Lett. XXXX, XXX, XXX−XXX

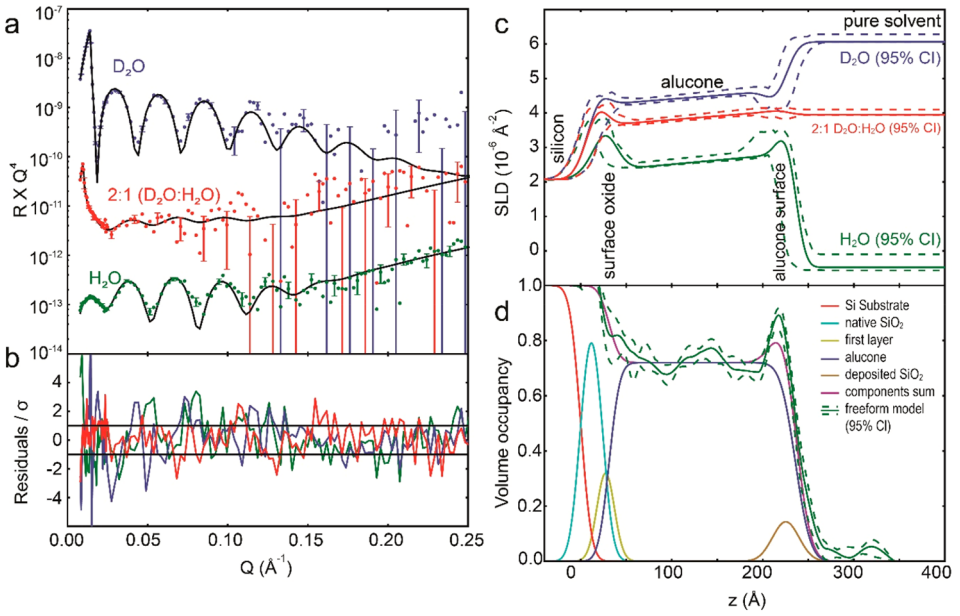

Figure 2. Neutron reflectivity of alucone on silicon. (a) Neutron reflectivity of alucone in buffers based on D_2O, H_2O, and a 2:1 mixture of D_2O/H_2O. Reflectivity is multiplied by Q_z^4, successive curves are offset by a factor of 10,[2] and error bars are shown sparsely for clarity. Error bars represent 68% confidence intervals arising from Poisson counting uncertainty. (b) Residuals of volume occupancy model optimization to reflectivity curves. (c) SLD profiles of the alucone layer derived from the optimized volume occupancy model. Dashed lines are 95% confidence intervals. (d) The optimized underlying volume-occupancy model, showing good agreement with a free-form model (green curve; dashed lines are 95% confidence intervals or CI).

temperatures (125 and 150 °C) to manipulate inorganic structure in the films, which, in turn, affects the membrane porosity and film thickness per cycle. The thickness was measured using an ellipsometer (Rudolph Research AutoEL II), which revealed the deposition rate decreases with an increase in temperature. The result of film thickness as a function of the number of cycles is shown in Figure 1b.

The porosity of the alucone layer was characterized using neutron reflectometry (NR). A 20 nm layer of alucone was deposited on a 5 mm thick silicon wafer, followed by the deposition of a 2 nm SiO_2 layer, which has been found to improve layer stability while maintaining porosity. This oxide layer also allows us to functionalize the surface using silane chemistry (see SI Figure 5), necessary for sample immobilization on the membrane surface,[52] a necessary step in the sequencing assay. The alucone-coated wafer was mounted in an NR flow cell so that the alucone surface was in contact with a 100 μm thick reservoir. The flow cell was mounted on the MAGIK vertical neutron reflectometer at the National Institute for Standards and Technology (NIST) Center for Neutron Research (NCNR).[53] The reservoir was then filled with D_2O buffered at pH 8 with 50 mM tris(hydroxymethyl)-aminomethane, and the reflectivity from the sample was monitored until full hydration was achieved.

The reflectivity of the alucone-coated silicon surface to 5 Å neutrons, multiplied by Q_z^4 for clarity (see the Neutron Reflectometry section) is shown in Figure 2a. Model fits are shown as solid lines, while the residuals are displayed in Figure 2b. The corresponding scattering length density (SLD) profiles are shown in Figure 2c, while the underlying molecular composition is shown in Figure 2d. The model components include a native SiO_2 layer on the silicon surface, a dense "first layer" forming the interface between the alucone and the substrate, the alucone layer itself, and the SiO_2 deposited by ALD on the alucone surface. The volume fraction occupied by each component, as well as its material-specific SLD, were free parameters in the optimizations. The interfacial roughnesses are described by two additional parameters: one for the substrate-proximal layers and one for the components on the substrate-distal surface of the alucone. Important structural parameters are presented in Table 1. The water-accessible porosity of the alucone film is found to be 28%.

Table 1. Important Structural Parameters of Alucone[a]

parameter	value
alucone thickness	$204.7^{+4.1}_{-4.4}$ Å
water fraction in hydrated alucone	$0.284^{+0.011}_{-0.007}$
alucone rms[b] surface roughness	$9.3^{+5.1}_{-2.6}$ Å
average alucone SLD	$3.813^{+0.074}_{-0.040} \times 10^{-6}$ Å^{-2}

[a]Uncertainties are 95% confidence intervals. [b]rms = root-mean square.

Freestanding Alucone Membranes. To demonstrate the DNA-capturing ability of the freestanding porous layers, we prepared SiN membranes that contain a small region that has a free-standing alucone membrane (see the Fabrication section). This was achieved by deposition of an alucone film on a SiN membrane that has premade (3 μm wide) circular regions in which the SiN is thinner than the surrounding bulk membrane. Following deposition, the SiN membrane is back-etched using RIE until SiN in the circular regions is thoroughly removed, leaving a pair of 3 μm diameter freestanding conducting porous membranes on an otherwise multilayer nonconducting membrane (Figure 3a). We observe that 3 μm porous membranes maintain their structural integrity over time for at least 24 h. Next, the alucone membrane's PL was measured using a Renishaw Ramascope setup equipped with a 100× objective, and all spectra were measured using a 488 nm excitation laser. The PL spectra from the circular membranes

DOI: 10.1021/acs.nanolett.8b04170
Nano Lett. XXXX, XXX, XXX−XXX

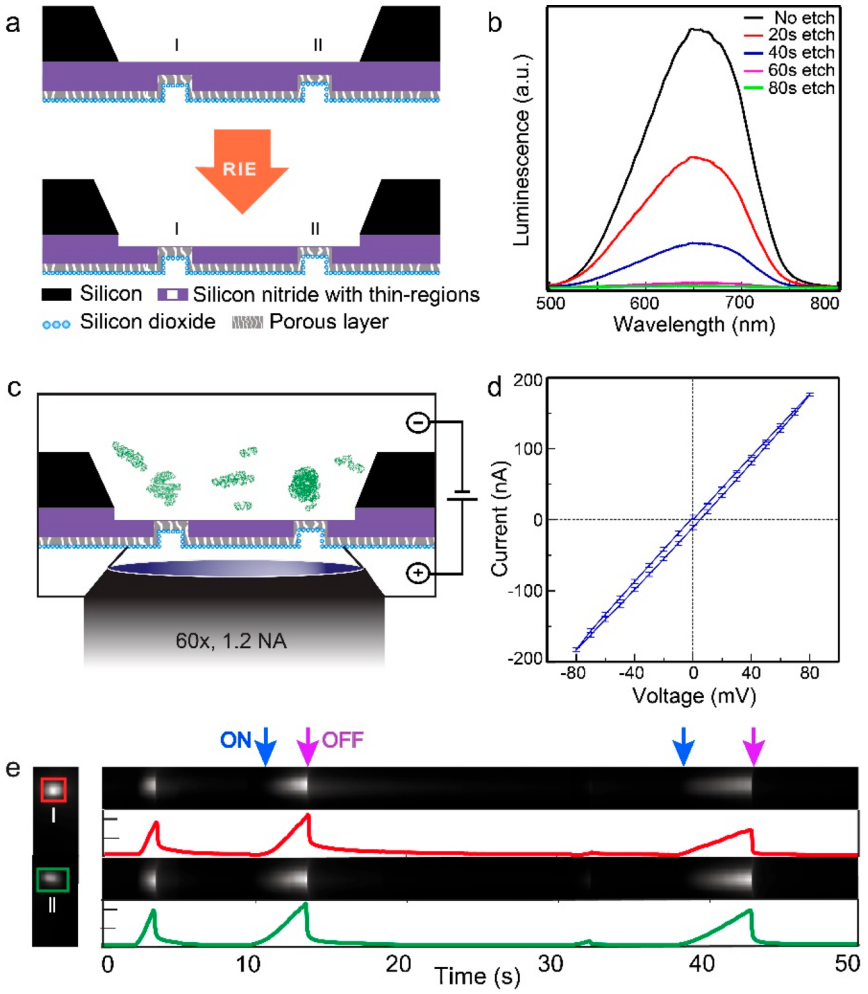

Figure 3. Experimental setup and DNA capture. (a) A Schematic of porous membrane on a free-standing SiN chip. The porous layer is deposited on top of the silicon nitride membrane, and back-etching the nitride exposes the thin porous region (shown as I and II). SiO_2 is deposited atop porous layer using ALD technique for better surface chemistry, low noise, and low background signal. (b) Photoluminescence spectrum of the porous layer before and after nitride thinning. (c) A porous thin-region chip mounted on a fluorescence microscope with an integrated Faraday cage and patch clamp amplifier and reimaged via a 60×, 1.2 NA water immersion objective. (d) The $I-V$ curve of the porous thin-region membrane in 10 mM KCl (error bars represent one standard deviation from 5 measurements). (e) The kymograph shows a time series of DNA capture in two thin regions (shown as I and II); red and green boxes show the area of interest. Images are projections of all frames before (ON) and after (OFF) the application of voltage during an experiment and are both of the same fluorescence-intensity scale. Fluorescence intensity traces from two different porous thin regions (red and green rectangles) is seen when a voltage is applied (ON). In the absence (OFF) of bias, DNA is not captured, and no fluorescence activity is observed.

before and after nitride thinning was measured. It can be seen from Figure 3b that upon thinning, the nitride the PL intensity continues to decrease. After etching of the entire SiN, the freestanding porous membrane emits a very weak PL signal, which makes it suitable for the detection of single-molecule fluorescence events for sequencing applications.

The necessary requirements for a porous membrane intended for DNA sequencing are porosity and conduction of ionic current, mechanical and chemical stability, and low photoluminescence (PL). To measure the membrane's conductance, capture DNA, and to record fluorescence burst from the tagged DNA, the membrane-supporting chip is mounted in a cell and placed in a Faraday cage on top of a fluorescence microscope that is coupled to a patch clamp amplifier, excitation lasers (blue, green, and red), and an imaging system[38] (Figure 3c). Applying a voltage bias across this membrane generates a localized electric field and electrophoretically draws charged molecules to the porous membranes. Figure 3d displays a current−voltage ($I-V$) curve measured with 10 mM KCl (10 mM Tris, 1 mM EDTA, pH 8). The linear $I-V$ curve indicates the membranes are porous enough to allow the ions to pass through them. The minor hysteresis observed is due to the capacitance from the porous structure. The conductance of the chip was measured over time for 4 h, and the average conductance during an experiment was observed to be 0.31 ± 0.218 $\mu S/\mu m^2$ (the error bar is one standard deviation from the mean). No electrochemical reaction was observed on the porous membrane, evidenced by the steady baseline current observed throughout the experiment. This chip was further used to demonstrate capture of picomolar concentrations of DNA. YOYO-1-stained DNA was prepared from 3500 bp DNA and YOYO-1 intercalating dye with a 10:1 base pair-to-dye molar ratio. A total of 10 pM of YOYO−DNA was loaded into the chamber, and membranes were continuously excited by a blue laser (488 nm). A 100 mV bias was applied across the

DOI: 10.1021/acs.nanolett.8b04170
Nano Lett. XXXX, XXX, XXX−XXX

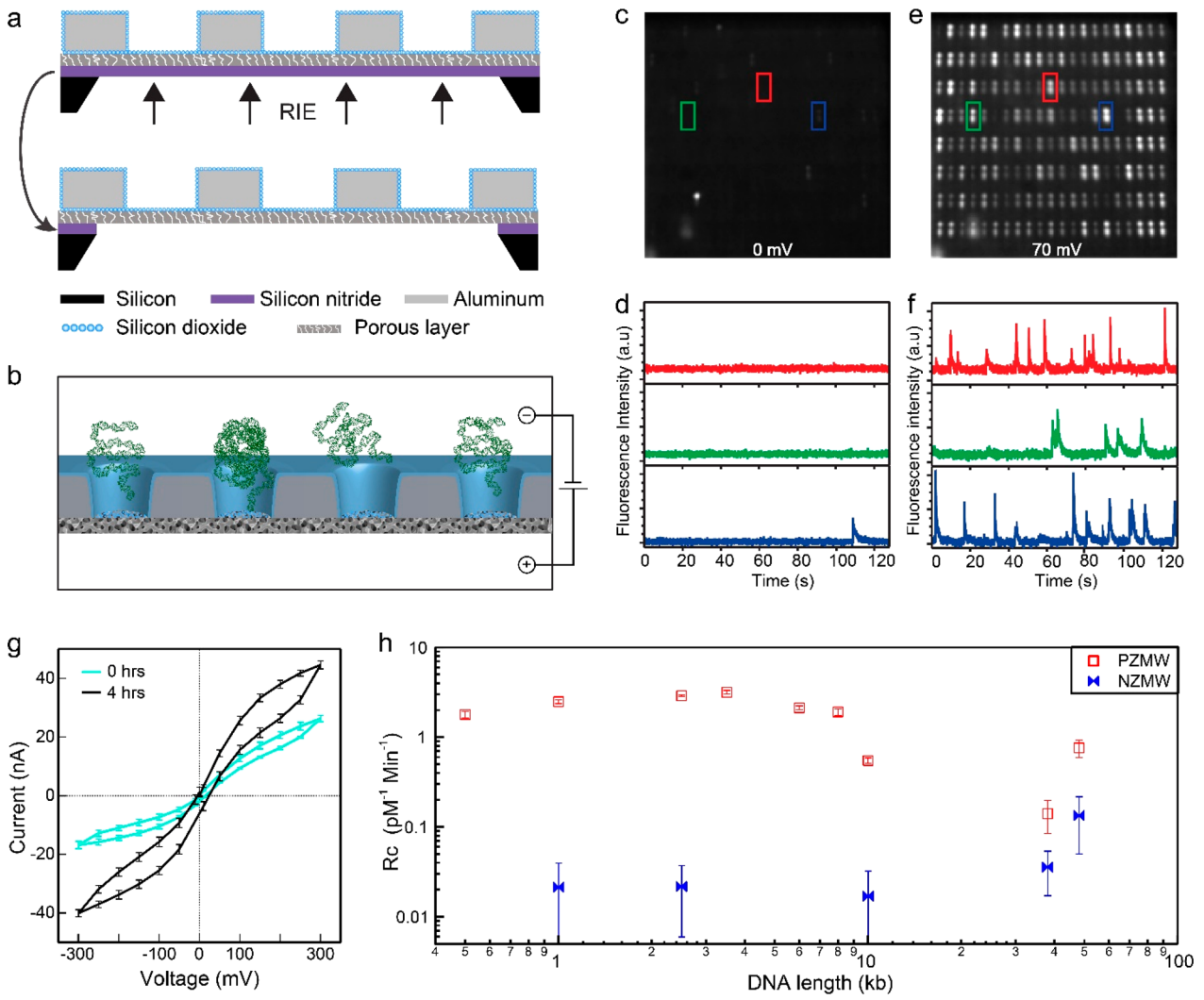

Figure 4. DNA loading using PZMW. (a) Scheme of the PZMW chip before and after etching silicon nitride. (b) Schematic representation of DNA loading on the cis side of the PZMW chip and applying a voltage bias. The panels represents an array of PZMWs in the same device during DNA loading at positive voltage bias. (c, d) An entire PZMW membrane (21 × 8 array), the image is a projection of all frames before applying voltage bias (0 mV). Red, green, and blue boxes show the area of interest for different PZMWs. The YOYO−DNAs were excited using 488 nm laser (5 mW laser power at objective plane, 60× water immersion), and the fluorescence traces from these PZMWs were recorded using emCCD over time are shown. In the absence of electric field, YOYO-I stained dsDNA are not captured (red and green traces), but over time, due to diffusion or voltage offset, DNA are seen to be captured (blue trace). (e, f) In the presence of applied voltage bias (70 mV), DNAs are immobilized in all of the PZMWs and is confirmed by the increase in the fluorescence intensity followed by photobleaching over time, captured using a emCCD camera and 60× objective lens. The intensity trace shows the activity of DNA capture in marked PZMWs. (g) $I-V$ curves of the a PZMW chip in 10 mM KCl before and after the experiment is shown (error bars represent 1 standard deviation from 10 measurements). (h) The capture rate of varying length of YOYO−DNA into PZMWs at 200 mV is plotted in units of millivolts per picomoles per minute (error bars represent 1 standard deviation) and is compared against the previously reported NZMW data[38] at V = 200 mV (error bars are 1 standard deviation).

membrane to electrophoretically load YOYO−DNA to each porous membrane. Figure 3e shows the kymograph of the fluorescence intensity in the areas of interest marked as I and II and indicated by red and green rectangles. When a voltage bias is applied (ON) (indicated by the blue arrow) the accumulation of YOYO−DNA at the porous regions is observed, as confirmed by the continuous increase in fluorescence intensity from the labeled DNAs. After the voltage is turned off (indicated by purple arrow), both of the porous regions show a drop in the fluorescence intensity level indicating DNA escape by diffusion. The porosity of the membrane enables ion transport across it, but due to the small pore size, DNA passage cannot take place, resulting in electrokinetic DNA trapping. After the experiment, the chip was stored in DI water and its conductance was measured again 24 h later. The conductance showed only a 5% increase, which confirmed the membrane is still stable and conductive.

Picogram DNA Capture Using Porous ZMWs. After the successful preliminary experiment of capturing labeled DNA molecules using porous membranes, ZMWs were fabricated as described previously,[38] on top of an alucone layer capped with SiO_2, deposited atop SiN layer on a 4 in. silicon wafer (see the Supporting Information). Briefly, we use electron-beam lithography and negative resist to make an array of 100 nm pillars in wafer scale. Next, we evaporate a 100 nm thick layer of aluminum on the wafer and use the lift-off technique to form the aluminum wells. After ZMWs are made, photolithography is performed on the back side of the wafer and nitride is etched

DOI: 10.1021/acs.nanolett.8b04170
Nano Lett. XXXX, XXX, XXX−XXX

selectively from the photo window. The back side of the silicon wafer is etched by KOH, and finally, the SiN layer is removed using RIE (Figure 4a), giving access to the porous layer within each ZMWs. This new device, called the porous ZMW (PZMW), contains an inorganic low-photoluminescence porous membrane that allows the electrokinetic capture of biomolecules (see the Supporting Information) in a facile and scalable manner. A schematic illustration of a PZMW device is shown in Figure 4b. A solution of 10 pM 10 kbp dsDNA-labeled YOYO-1 dye was used, and the change in fluorescence intensity as a function of time at each PZMW (21 × 8 array) was recorded using an emCCD camera. In the absence of voltage bias (0 mV), no activity is seen at the base of PZMWs, indicated by red, green, and blue boxes (Figures 4c,d). Nonetheless, DNA capture is observed over time in a few PZMWs, owing to the diffusion loading and possibly an existing voltage offset. Applying a voltage bias (70 mV) across the PZMW membrane resulted in electrophoretic focusing of individual YOYO-1-stained DNA molecules within the illumination volume of PZMWs, where the DNA molecules are excited using a blue laser. The DNA loaded PZMWs are visible with notable fluorescence bursts (Figure 4e). Figure 4f shows distinct entry of individual DNA molecules into the PZMWs, as indicated by the intensity spikes after each capture followed by photobleaching over time. Each molecule stays in the waveguide for specified time before it escapes by diffusion. The fluorescence traces from all PZMWs are shown in Figure S2. Throughout the experiment, the steady capture of DNA molecules was observed for an extended time (>8 h). This indicates that DNA neither accumulates in the waveguides nor irreversibly blocks the entrances to the porous network. PZMW chips can successfully be reused after a day for DNA capturing. In Figure 4g, $I-V$ curves of the PZMW chip before and after the experiment are shown. An increase in conductance over time was observed indicating continuous disintegration of the organic compound in the alucone during the experiment. The average conductance after the experiment was observed to be 0.20 ± 0.09 $\mu S/\mu m^2$. Here, conductance was obtained by fitting a line to the $I-V$ curves below 50 mV (the linear regime) and averaging over 10 measurements (error represent are one standard deviation from 10 measurements). The nonlinear $I-V$ curve above 100 mV suggests concentration polarization[54] at the porous membrane, which limits ion transport at higher voltages.

The capture rate of DNA molecules in the picomolar concentration range as a function of DNA length, from 500 bp to 48 kbp, was measured using the PZMWs. In these experiments, the concentration of DNA molecules shorter than 10 kbp was 10 pM, and a 1 pM concentration was used for molecules equal to or longer than 10 kbp. The experiments were carried out at 200 mV applied bias, and the interspike duration for different DNA lengths in each PZMWs was measured from which the capture rates (R_c) were calculated. The capture rates normalized by DNA concentration are presented in Figure 4h and compared with our previously reported DNA capture data using NZMWs,[38] which were measured under the same experimental conditions (V = 200 mV). DNA packaging in nanometer size geometric confinements, such as virus capsids, requires substantial energy to overcome the entropic barriers during DNA compression. In this case, the electric field applied across the PZMW membrane provides the energy required for DNA packing. The capture rate of PZMWs is only slightly dependent on DNA length. PZMWs display at least 1 order of magnitude (2 for shorter molecules) of enhancement in capture rate over the NZMWs across the entire range of tested DNAs. We note that the capture trend observed for NZMWs and PZMWs for increasing DNA lengths appears to have opposite trends: whereas there is a slight increase for longer DNA molecules in the case of NZMWs, for PZMWs, there is an apparent decrease. These noticeable and opposite trends may be somewhat skewed by the fact that capture of DNA into NZMWs and PZMWs have fundamentally different fates: while in NZMWs, there is a finite possibility of eventual translocation, in PZMWs, this is not possible because the small and tortuous pore structure does not allow DNA to traverse the membrane. Therefore, capture is negatively skewed by the fact that PZMW occupancy precludes the capture of other molecules, whereas in NZMWs, there is a sink provided by translocation.

In summary, we have successfully demonstrated second-generation ZMW devices that consist of a porous membrane at the base of each ZMW for efficient loading of single molecules from small input quantities. These devices are stable and can be used for more than 1 day. Combining ZMWs with a porous membrane allows the low-cost fabrication of these devices at the wafer scale without a need for techniques such as transmission electron microscopy to drill a nanopore at the base of each ZMW. The electrokinetic capture of YOYO−DNA reveals loading rates independent of DNA length, while we expect that other biomolecules can also be captured in a facile and scalable manner. PZMWs provide ion-conductive pathways across the entire membrane in the form of tortuous and straight channels and effectively immobilize the sequencing molecule at their base. We have also demonstrated that silane chemistry can be used to immobilize labeled streptavidin, laying the groundwork for future work focused on parallelizing low-input DNA sequencing. We have demonstrated that these PZMW devices can be used with an existing DNA sequencing setup and is a replacement for our previously reported NZMW devices for SMRT sequencing.

Experimental Details of Neutron Reflectometry. For reflectivity measurements, a monochromatic beam of wavelength 5 Å impinged on the interface between the coated surface of the sample wafer and the liquid in a 100 μm thick reservoir. The pre-sample collimating slits were chosen to maintain a constant illuminated interfacial area for each measured angle θ. The post-sample collimation was chosen to allow the entire reflected beam to impinge on the detector, which was positioned at an angle 2θ relative to the incoming beam direction to measure specular reflection. Each reflectivity curve covered a range in scattering vector $Q_z = 4\pi\lambda^{-1} \sin(\theta)$ from 0.008 to 0.25 $Å^{-1}$.

The reflectivity was calculated as $R = (I(Q_z) - I_B(Q_z))/I_0(Q_z)$, where $I(Q_z)$ is the measured count rate (normalized to a much larger monitor count rate to account for fluctuations in beam intensity). $I_B(Q_z)$ is the background intensity, which arises primarily from incoherent scattering from the liquid reservoir and is calculated by linear interpretation of the intensities measured with the detector positioned at 1.5θ and 2.5θ. $I_0(Q_z)$ is the incident-beam intensity (also normalized to the monitor count rate) and is directly measured through the silicon substrate at $\theta = 0$ with the detector positioned in line with the incident beam.

To reconstruct the SLD profile of the alucone, NR data were collected in buffer solutions using three aqueous solvents: D_2O

DOI: 10.1021/acs.nanolett.8b04170
Nano Lett. XXXX, XXX, XXX−XXX

(SLD of 6.33×10^{-6} Å^{-2}), H_2O (SLD of -0.56×10^{-6} Å^{-2}), and a 2:1 mixture of D_2O and H_2O (SLD of 4.03×10^{-6} Å^{-2}). Differences in the SLD profiles of the alucone-coated surface in different solvents gives information about the volume occupancy of the aqueous medium in the alucone layer. NR data were modeled using the composition space modeling procedures described previously.[55] Simultaneous optimization of the composition space model for the three solvent conditions was performed on the Bridges[56,57] high-performance computing system using the DREAM Markov Chain Monte Carlo algorithm[58] implemented in the software package Bumps.[59] Confidence intervals on parameters and model predictions were calculated from sparse sampling of 2.9 million DREAM samples after the optimizer had reached steady state. The optimization achieved a reduced χ^2 of 2.1.

Fabrication. The SiN membranes with locally thinned circular regions were made by deposition of 50 nm low-stress SiN on 500 μm thick silicon wafers. Next, using photolithography, 3 μm diameter circular regions separated by 25 μm each were masked on one side of the silicon wafer. After development, 20 nm of SiN from circular regions was removed using RIE. Later, the other side of the wafer was masked using square photo windows separated by 5 mm each and developed, and SiN was removed from square photo windows followed by etching of the silicon wafer in the <100> plane by KOH at 65 °C, leaving behind a SiN membrane with a pair of 3 μm circular regions.

Sample Preparation. YOYO-labeled dsDNA was prepared using either λ-DNA or NoLimits dsDNA fragments (ThermoFisher Scientific) of different lengths (500 bp to 20 kbp) and YOYO-1 intercalating dye (Life Technologies, Carlsbad, CA). dsDNA and YOYO-1 dye were mixed together at 10:1 (base pair/dye) molar ratio and incubated for 20 min at 50 °C.

■ ASSOCIATED CONTENT

Supporting Information

The Supporting Information is available free of charge on the ACS Publications website at DOI: 10.1021/acs.nanolett.8b04170.

Additional details of the fabrication process for porous zero-mode waveguides, YOYO−DNA capture fluorescence traces, analysis of DNA capture data, capture rates of non-DNA biomolecules, and a comparison of loading rates into NZMWs and PZMWs (PDF)

■ AUTHOR INFORMATION

Corresponding Author

*E-mail: wanunu@northeastern.edu.

ORCID

David P. Hoogerheide: 0000-0003-2918-1469

Meni Wanunu: 0000-0002-9837-0004

Notes

The authors declare no competing financial interest.

■ ACKNOWLEDGMENTS

We thank Dr. Mohammad Amin Alibakhshi and Dr. Joseph Larkin for proof reading the manuscript, Dr. Robert Y. Henley for Python programming of the optical analysis software, and Hannah Bialic for initial characterization of the porous membrane properties. We thank Prof. Barry S. Cooperman, Department of Chemistry, University of Pennsylvania for providing the labeled ribosome sample. This research work was supported by NIH: NHGRI award no 1R01 HG009186 (MW and JK). We acknowledge staff from Cornell NanoScale Science and Technology Facility, for useful advice in fabrication. This work was performed in part at the Cornell NanoScale Facility (CNF), a member of the National Nanotechnology Coordinated Infrastructure (NNCI), which is supported by the National Science Foundation (Grant ECCS-1542081). We acknowledge the National Institute of Standards and Technology, U.S. Department of Commerce, for providing the neutron research facilities used in this work. This work used the Extreme Science and Engineering Discovery Environment (XSEDE), which is supported by National Science Foundation grant number ACI-1053575. Specifically, it used the Bridges system, which is supported by NSF award number ACI-1445606, at the Pittsburgh Supercomputing Center (PSC). Certain commercial materials, equipment, and instruments are identified in this work to describe the experimental procedure as completely as possible. In no case does such an identification imply a recommendation or endorsement by NIST, nor does it imply that the materials, equipment, or instruments identified are necessarily the best available for the purpose.

■ REFERENCES

(1) Sanger, F.; Nicklen, S.; Coulson, A. R. *Proc. Natl. Acad. Sci. U. S. A.* **1977**, *74*, 5463−7.

(2) Rothberg, J. M.; Leamon, J. H. *Nat. Biotechnol.* **2008**, *26*, 1117−24.

(3) Eid, J.; Fehr, A.; Gray, J.; Luong, K.; Lyle, J.; Otto, G.; Peluso, P.; Rank, D.; Baybayan, P.; Bettman, B.; Bibillo, A.; Bjornson, K.; Chaudhuri, B.; Christians, F.; Cicero, R.; Clark, S.; Dalal, R.; Dewinter, A.; Dixon, J.; Foquet, M.; Gaertner, A.; Hardenbol, P.; Heiner, C.; Hester, K.; Holden, D.; Kearns, G.; Kong, X.; Kuse, R.; Lacroix, Y.; Lin, S.; Lundquist, P.; Ma, C.; Marks, P.; Maxham, M.; Murphy, D.; Park, I.; Pham, T.; Phillips, M.; Roy, J.; Sebra, R.; Shen, G.; Sorenson, J.; Tomaney, A.; Travers, K.; Trulson, M.; Vieceli, J.; Wegener, J.; Wu, D.; Yang, A.; Zaccarin, D.; Zhao, P.; Zhong, F.; Korlach, J.; Turner, S. *Science* **2009**, *323*, 133−8.

(4) Levy, S. E.; Myers, R. M. *Annu. Rev. Genomics Hum. Genet.* **2016**, *17*, 95−115.

(5) Zhou, B.; Donnelly, M. E.; Scholes, D. T.; St George, K.; Hatta, M.; Kawaoka, Y.; Wentworth, D. E. *J. Virol.* **2009**, *83*, 10309.

(6) Kellis, M.; Wold, B.; Snyder, M. P.; Bernstein, B. E.; Kundaje, A.; Marinov, G. K.; Ward, L. D.; Birney, E.; Crawford, G. E.; Dekker, J.; Dunham, I.; Elnitski, L. L.; Farnham, P. J.; Feingold, E. A.; Gerstein, M.; Giddings, M. C.; Gilbert, D. M.; Gingeras, T. R.; Green, E. D.; Guigo, R.; Hubbard, T.; Kent, J.; Lieb, J. D.; Myers, R. M.; Pazin, M. J.; Ren, B.; Stamatoyannopoulos, J. A.; Weng, Z.; White, K. P.; Hardison, R. C. *Proc. Natl. Acad. Sci. U. S. A.* **2014**, *111*, 6131−8.

(7) Wang, J.; Wang, W.; Li, R.; Li, Y.; Tian, G.; Goodman, L.; Fan, W.; Zhang, J.; Li, J.; Zhang, J.; Guo, Y.; Feng, B.; Li, H.; Lu, Y.; Fang, X.; Liang, H.; Du, Z.; Li, D.; Zhao, Y.; Hu, Y.; Yang, Z.; Zheng, H.; Hellmann, I.; Inouye, M.; Pool, J.; Yi, X.; Zhao, J.; Duan, J.; Zhou, Y.; Qin, J.; Ma, L.; Li, G.; Yang, Z.; Zhang, G.; Yang, B.; Yu, C.; Liang, F.; Li, W.; Li, S.; Li, D.; Ni, P.; Ruan, J.; Li, Q.; Zhu, H.; Liu, D.; Lu, Z.; Li, N.; Guo, G.; Zhang, J.; Ye, J.; Fang, L.; Hao, Q.; Chen, Q.; Liang, Y.; Su, Y.; San, A.; Ping, C.; Yang, S.; Chen, F.; Li, L.; Zhou, K.; Zheng, H.; Ren, Y.; Yang, L.; Gao, Y.; Yang, G.; Li, Z.; Feng, X.; Kristiansen, K.; Wong, G. K.; Nielsen, R.; Durbin, R.; Bolund, L.; Zhang, X.; Li, S.; Yang, H.; Wang, J. *Nature* **2008**, *456*, 60−5.

(8) Aird, D.; Ross, M. G.; Chen, W. S.; Danielsson, M.; Fennell, T.; Russ, C.; Jaffe, D. B.; Nusbaum, C.; Gnirke, A. *Genome Biol.* **2011**, *12*, R18.

DOI: 10.1021/acs.nanolett.8b04170
Nano Lett. XXXX, XXX, XXX−XXX

(9) Larsen, P. A.; Heilman, A. M.; Yoder, A. D. *BMC Genomics* **2014**, *15*, 720.
(10) Simpson, J. T.; Workman, R. E.; Zuzarte, P. C.; David, M.; Dursi, L. J.; Timp, W. *Nat. Methods* **2017**, *14*, 407−410.
(11) Flusberg, B. A.; Webster, D. R.; Lee, J. H.; Travers, K. J.; Olivares, E. C.; Clark, T. A.; Korlach, J.; Turner, S. W. *Nat. Methods* **2010**, *7*, 461−5.
(12) Clarke, J.; Wu, H. C.; Jayasinghe, L.; Patel, A.; Reid, S.; Bayley, H. *Nat. Nanotechnol.* **2009**, *4*, 265−70.
(13) Jain, M.; Olsen, H. E.; Paten, B.; Akeson, M. *Genome Biol.* **2016**, *17*, 239.
(14) Jain, M.; Koren, S.; Miga, K. H.; Quick, J.; Rand, A. C.; Sasani, T. A.; Tyson, J. R.; Beggs, A. D.; Dilthey, A. T.; Fiddes, I. T.; Malla, S.; Marriott, H.; Nieto, T.; O'Grady, J.; Olsen, H. E.; Pedersen, B. S.; Rhie, A.; Richardson, H.; Quinlan, A. R.; Snutch, T. P.; Tee, L.; Paten, B.; Phillippy, A. M.; Simpson, J. T.; Loman, N. J.; Loose, M. *Nat. Biotechnol.* **2018**, *36*, 338−345.
(15) Loman, N. J.; Quick, J.; Simpson, J. T. *Nat. Methods* **2015**, *12*, 733−5.
(16) Ashton, P. M.; Nair, S.; Dallman, T.; Rubino, S.; Rabsch, W.; Mwaigwisya, S.; Wain, J.; O'Grady, J. *Nat. Biotechnol.* **2015**, *33*, 296−300.
(17) Quick, J.; Loman, N. J.; Duraffour, S.; Simpson, J. T.; Severi, E.; Cowley, L.; Bore, J. A.; Koundouno, R.; Dudas, G.; Mikhail, A.; Ouedraogo, N.; Afrough, B.; Bah, A.; Baum, J. H.; Becker-Ziaja, B.; Boettcher, J. P.; Cabeza-Cabrerizo, M.; Camino-Sanchez, A.; Carter, L. L.; Doerrbecker, J.; Enkirch, T.; Dorival, I. G. G.; Hetzelt, N.; Hinzmann, J.; Holm, T.; Kafetzopoulou, L. E.; Koropogui, M.; Kosgey, A.; Kuisma, E.; Logue, C. H.; Mazzarelli, A.; Meisel, S.; Mertens, M.; Michel, J.; Ngabo, D.; Nitzsche, K.; Pallasch, E.; Patrono, L. V.; Portmann, J.; Repits, J. G.; Rickett, N. Y.; Sachse, A.; Singethan, K.; Vitoriano, I.; Yemanaberhan, R. L.; Zekeng, E. G.; Racine, T.; Bello, A.; Sall, A. A.; Faye, O.; Faye, O.; Magassouba, N.; Williams, C. V.; Amburgey, V.; Winona, L.; Davis, E.; Gerlach, J.; Washington, F.; Monteil, V.; Jourdain, M.; Bererd, M.; Camara, A.; Somlare, H.; Camara, A.; Gerard, M.; Bado, G.; Baillet, B.; Delaune, D.; Nebie, K. Y.; Diarra, A.; Savane, Y.; Pallawo, R. B.; Gutierrez, G. J.; Milhano, N.; Roger, I.; Williams, C. J.; Yattara, F.; Lewandowski, K.; Taylor, J.; Rachwal, P.; Turner, D.; Pollakis, G.; Hiscox, J. A.; Matthews, D. A.; O'Shea, M. K.; Johnston, A. M.; Wilson, D.; Hutley, E.; Smit, E.; Di Caro, A.; Woelfel, R.; Stoecker, K.; Fleischmann, E.; Gabriel, M.; Weller, S. A.; Koivogui, L.; Diallo, B.; Keita, S.; Rambaut, A.; Formenty, P.; Gunther, S.; Carroll, M. W. *Nature* **2016**, *530*, 228−232.
(18) Jain, M.; Olsen, H. E.; Turner, D. J.; Stoddart, D.; Bulazel, K. V.; Paten, B.; Haussler, D.; Willard, H. F.; Akeson, M.; Miga, K. H. *Nat. Biotechnol.* **2018**, *36*, 321−323.
(19) Kuderna, L. F. K.; Lizano, E.; Julia, E.; Gomez-Garrido, J.; Serres-Armero, A.; Kuhlwilm, M.; Antoni Alandes, R.; Alvarez-Estape, M.; Alioto, T.; Gut, M.; Gut, I.; Heide Schierup, M.; Fornas, O.; Marques-Bonet, T. Selective single molecule sequencing and assembly of a human Y chromosome of African origin. *bioRxiv* **2018**, 1.
(20) Levene, M. J.; Korlach, J.; Turner, S. W.; Foquet, M.; Craighead, H. G.; Webb, W. W. *Science* **2003**, *299*, 682−6.
(21) Foquet, M.; Samiee, K. T.; Kong, X. X.; Chauduri, B. P.; Lundquist, P. M.; Turner, S. W.; Freudenthal, J.; Roitman, D. B. *J. Appl. Phys.* **2008**, *103*, No. 034301.
(22) Rhoads, A.; Au, K. F. *Genomics, Proteomics Bioinf.* **2015**, *13*, 278−89.
(23) Gordon, D.; Huddleston, J.; Chaisson, M. J.; Hill, C. M.; Kronenberg, Z. N.; Munson, K. M.; Malig, M.; Raja, A.; Fiddes, I.; Hillier, L. W.; Dunn, C.; Baker, C.; Armstrong, J.; Diekhans, M.; Paten, B.; Shendure, J.; Wilson, R. K.; Haussler, D.; Chin, C. S.; Eichler, E. E. *Science* **2016**, *352*, aae0344.
(24) Chaisson, M. J.; Huddleston, J.; Dennis, M. Y.; Sudmant, P. H.; Malig, M.; Hormozdiari, F.; Antonacci, F.; Surti, U.; Sandstrom, R.; Boitano, M.; Landolin, J. M.; Stamatoyannopoulos, J. A.; Hunkapiller, M. W.; Korlach, J.; Eichler, E. E. *Nature* **2015**, *517*, 608−11.
(25) Berlin, K.; Koren, S.; Chin, C. S.; Drake, J. P.; Landolin, J. M.; Phillippy, A. M. *Nat. Biotechnol.* **2015**, *33*, 623−30.
(26) Koren, S.; Harhay, G. P.; Smith, T. P.; Bono, J. L.; Harhay, D. M.; McVey, S. D.; Radune, D.; Bergman, N. H.; Phillippy, A. M. *Genome Biol.* **2013**, *14*, R101.
(27) Lan, T.; Renner, T.; Ibarra-Laclette, E.; Farr, K. M.; Chang, T. H.; Cervantes-Perez, S. A.; Zheng, C.; Sankoff, D.; Tang, H.; Purbojati, R. W.; Putra, A.; Drautz-Moses, D. I.; Schuster, S. C.; Herrera-Estrella, L.; Albert, V. A. *Proc. Natl. Acad. Sci. U. S. A.* **2017**, *114*, E4435−E4441.
(28) Teh, B. T.; Lim, K.; Yong, C. H.; Ng, C. C. Y.; Rao, S. R.; Rajasegaran, V.; Lim, W. K.; Ong, C. K.; Chan, K.; Cheng, V. K. Y.; Soh, P. S.; Swarup, S.; Rozen, S. G.; Nagarajan, N.; Tan, P. *Nat. Genet.* **2017**, *49*, 1633−1641.
(29) Jiao, Y.; Peluso, P.; Shi, J.; Liang, T.; Stitzer, M. C.; Wang, B.; Campbell, M. S.; Stein, J. C.; Wei, X.; Chin, C. S.; Guill, K.; Regulski, M.; Kumari, S.; Olson, A.; Gent, J.; Schneider, K. L.; Wolfgruber, T. K.; May, M. R.; Springer, N. M.; Antoniou, E.; McCombie, W. R.; Presting, G. G.; McMullen, M.; Ross-Ibarra, J.; Dawe, R. K.; Hastie, A.; Rank, D. R.; Ware, D. *Nature* **2017**, *546*, 524−527.
(30) Pendleton, M.; Sebra, R.; Pang, A. W.; Ummat, A.; Franzen, O.; Rausch, T.; Stutz, A. M.; Stedman, W.; Anantharaman, T.; Hastie, A.; Dai, H.; Fritz, M. H.; Cao, H.; Cohain, A.; Deikus, G.; Durrett, R. E.; Blanchard, S. C.; Altman, R.; Chin, C. S.; Guo, Y.; Paxinos, E. E.; Korbel, J. O.; Darnell, R. B.; McCombie, W. R.; Kwok, P. Y.; Mason, C. E.; Schadt, E. E.; Bashir, A. *Nat. Methods* **2015**, *12*, 780−6.
(31) Chaisson, M. J.; Wilson, R. K.; Eichler, E. E. *Nat. Rev. Genet.* **2015**, *16*, 627−40.
(32) Shi, L.; Guo, Y.; Dong, C.; Huddleston, J.; Yang, H.; Han, X.; Fu, A.; Li, Q.; Li, N.; Gong, S.; Lintner, K. E.; Ding, Q.; Wang, Z.; Hu, J.; Wang, D.; Wang, F.; Wang, L.; Lyon, G. J.; Guan, Y.; Shen, Y.; Evgrafov, O. V.; Knowles, J. A.; Thibaud-Nissen, F.; Schneider, V.; Yu, C. Y.; Zhou, L.; Eichler, E. E.; So, K. F.; Wang, K. *Nat. Commun.* **2016**, *7*, 12065.
(33) Seo, J. S.; Rhie, A.; Kim, J.; Lee, S.; Sohn, M. H.; Kim, C. U.; Hastie, A.; Cao, H.; Yun, J. Y.; Kim, J.; Kuk, J.; Park, G. H.; Kim, J.; Ryu, H.; Kim, J.; Roh, M.; Baek, J.; Hunkapiller, M. W.; Korlach, J.; Shin, J. Y.; Kim, C. *Nature* **2016**, *538*, 243−247.
(34) Huddleston, J.; Chaisson, M. J. P.; Steinberg, K. M.; Warren, W.; Hoekzema, K.; Gordon, D.; Graves-Lindsay, T. A.; Munson, K. M.; Kronenberg, Z. N.; Vives, L.; Peluso, P.; Boitano, M.; Chin, C. S.; Korlach, J.; Wilson, R. K.; Eichler, E. E. *Genome Res.* **2017**, *27*, 677−685.
(35) Sedlazeck, F. J.; Rescheneder, P.; Smolka, M.; Fang, H.; Nattestad, M.; von Haeseler, A.; Schatz, M. C. *Nat. Methods* **2018**, *15*, 461−468.
(36) *Pacific Biosciences Template Preparation and Sequencing Guide*; Pacific Biosciences of California: Menlo Park, CA, 2014.
(37) Larkin, J.; Foquet, M.; Turner, S. W.; Korlach, J.; Wanunu, M. *Nano Lett.* **2014**, *14*, 6023−9.
(38) Larkin, J.; Henley, R. Y.; Jadhav, V.; Korlach, J.; Wanunu, M. *Nat. Nanotechnol.* **2017**, *12*, 1169−1175.
(39) Kim, M. J.; Wanunu, M.; Bell, D. C.; Meller, A. *Adv. Mater.* **2006**, *18*, 3149.
(40) Yang, J.; Ferranti, D. C.; Stern, L. A.; Sanford, C. A.; Huang, J.; Ren, Z.; Qin, L. C.; Hall, A. R. *Nanotechnology* **2011**, *22*, 285310.
(41) Ahmadi, A. G.; Nair, S. *Microelectron. Eng.* **2013**, *112*, 149−156.
(42) Sawafta, F.; Clancy, B.; Carlsen, A. T.; Huber, M.; Hall, A. R. *Nanoscale* **2014**, *6*, 6991−6.
(43) Zhang, M.; Schmidt, T.; Jemt, A.; Sahlen, P.; Sychugov, I.; Lundeberg, J.; Linnros, J. *Nanotechnology* **2015**, *26*, 314002.
(44) Verschueren, D. V.; Yang, W.; Dekker, C. *Nanotechnology* **2018**, *29*, 145302.
(45) Wang, Y.; Ying, C.; Zhou, W.; de Vreede, L.; Liu, Z.; Tian, J. *Sci. Rep.* **2018**, *8*, 1234.
(46) Auger, T.; Bourhis, E.; Donnez, J.; Durnez, A.; Di Meglio, J. M.; Auvray, L.; Montel, F.; Yates, J.; Gierak, J. *Microelectron. Eng.* **2018**, *187*, 90−94.

DOI: 10.1021/acs.nanolett.8b04170
Nano Lett. XXXX, XXX, XXX−XXX

(47) McMahon, C. N.; Alemany, L.; Callender, R. L.; Bott, S. G.; Barron, A. R. *Chem. Mater.* **1999**, *11*, 3181−3188.
(48) Dameron, A. A.; Seghete, D.; Burton, B. B.; Davidson, S. D.; Cavanagh, A. S.; Bertrand, J. A.; George, S. M. *Chem. Mater.* **2008**, *20*, 3315−3326.
(49) George, S. M.; Yoon, B.; Dameron, A. A. *Acc. Chem. Res.* **2009**, *42*, 498−508.
(50) Miller, D. C.; Foster, R. R.; Jen, S. H.; Bertrand, J. A.; Seghete, D.; Yoon, B.; Lee, Y. C.; George, S. M.; Dunn, M. L. *Acta Mater.* **2009**, *57*, 5083−5092.
(51) Liang, X. H.; Evanko, B. W.; Izar, A.; King, D. M.; Jiang, Y. B.; Weimer, A. W. *Microporous Mesoporous Mater.* **2013**, *168*, 178−182.
(52) Korlach, J.; Marks, P. J.; Cicero, R. L.; Gray, J. J.; Murphy, D. L.; Roitman, D. B.; Pham, T. T.; Otto, G. A.; Foquet, M.; Turner, S. W. *Proc. Natl. Acad. Sci. U. S. A.* **2008**, *105*, 1176−81.
(53) Dura, J. A.; Pierce, D. J.; Majkrzak, C. F.; Maliszewskyj, N. C.; McGillivray, D. J.; Losche, M.; O'Donovan, K. V.; Mihailescu, M.; Perez-Salas, U.; Worcester, D. L.; White, S. H. *Rev. Sci. Instrum.* **2006**, *77*, 74301.
(54) Kim, S. J.; Wang, Y. C.; Lee, J. H.; Jang, H.; Han, J. *Phys. Rev. Lett.* **2007**, *99*, No. 044501.
(55) Shekhar, P.; Nanda, H.; Losche, M.; Heinrich, F. J. *J. Appl. Phys.* **2011**, *110*, 102216−10221612.
(56) Nystrom, N. A.; Levine, M. J.; Roskies, R. Z.; Scott, J. R. Bridges. In *Proceedings of the 2015 XSEDE Conference on Scientific Advancements Enabled by Enhanced Cyberinfrastructure*; ACM: Saint Louis, MI, 2015; pp 1−8.
(57) Towns, J.; Cockerill, T.; Dahan, M.; Foster, I.; Gaither, K.; Grimshaw, A.; Hazlewood, V.; Lathrop, S.; Lifka, D.; Peterson, G. D.; Roskies, R.; Scott, J. R.; Wilkens-Diehr, N. *Comput. Sci. Eng.* **2014**, *16*, 62−74.
(58) Vrugt, J. A.; ter Braak, C. J. F.; Diks, C. G. H.; Robinson, B. A.; Hyman, J. M.; Higdon, D. *Int. J. Nonlinear Sci. Numer. Simul.* **2009**, *10*, 273−290.
(59) Kienzle, P. A.; Krycka, J.; Patel, N.; Sahin, I. Bumps, version *0.7.5.4*; University of Maryland: College Park, MD, 2011.

DOI: 10.1021/acs.nanolett.8b04170
Nano Lett. XXXX, XXX, XXX−XXX